Int J Ind Chem (2015) 6:247–259
DOI 10.1007/s40090-015-0046-8

RESEARCH

Electrocatalytic properties of polyaniline–TiO_2 nanocomposites

P. Rajakani[1] · **C. Vedhi**[1]

Received: 9 January 2015 / Accepted: 2 July 2015 / Published online: 1 September 2015

Abstract An efficient methodology of polyaniline–TiO_2 nancomposite (PAniTNC) was developed through various proportions of ceramic added by chemical polymerization at room temperature. The chemical polymerization reactions were carried out using potassium perdisulphate as an oxidizing agent. The particle size of PAniTNC was found in the range of 8–15 nm as analysed by transmission electron microscopy. The Ti–O characteristic stretching bands at 630 and 558 cm^{-1}, indicating the presence of TiO_2 in polyaniline matrix was confirmed by fourier transform infrared spectroscopy. The characterization of the nanocomposite crystalline shape was carried out using X-ray diffraction method. Thermogravimetric and differential scanning calorimetry analyses indicate high thermal stability. SEM analysis showed mixed granular nature of the polymer–ceramic nanocomposites. EDX analysis shows the presence of Ti, C and N in composites. Cyclic voltammetric studies exhibit good adherent behaviour on the electrode surface at pH 1.0. It reveals the presence of oxidation peak at 0.417 V and reduction peak at 0.285 V. It has been observed that PAniTNC-modified GCE has good oxygen reduction ability, and also enhances methanol reduction.

Keywords Polyaniline–TiO_2 nanocomposites · Voltammetry · TGA/DTA · SEM · TEM · XRD

✉ C. Vedhi
cvedhi@rediffmail.com; chinavedhi@yahoo.co.in

[1] Department of Chemistry, V.O Chidambaram College, Tuticorin, Tamil Nadu 628008, India

Introduction

Several approaches are developed in the recent years for full substitution of platinum in oxygen reduction reaction (ORR) electrocatalysts [1]. It is known that conducting polymers (CPs) such as polyaniline and polypyrrole can directly demonstrate electrocatalytic properties in ORR [2, 3], which is attractive for the development of ORR electrocatalysts on their basis. To enhance catalytic efficiency of CPs in ORR, it is suggested [4, 5] to use Keggin-type heteropoly acids (HPAs) for molecular dispersion of catalytically active particles as specific polymer dopants in the CP matrix.

It was found earlier [6, 7] that three-component nanocomposites are based on CPs (PAni or PPy), HPA and V_2O_5–CP HPA/V_2O_5, and their bifunctional analogues. Nanosize platinum containing CP HPA/V_2O_5/Pt single material and the properties of both CP HPA/V_2O_5 and CP/Pt composites show high electrocatalytic activity in ORR which is due to nanostructuring and interaction between the components. With account for this, it was of interest to elucidate the possibility of using other nanosize transition metal oxides for development of hybrid CP-based nanocomposites capable of manifesting electrocatalytic properties in ORR. Titanium dioxide featuring catalytic activity in a number of chemical, electrochemical and photochemical redox processes attracted our attention which eventually led to the development of metal oxide component with CP-based nanocomposites. In particular [8–10], various TiO_2 forms can demonstrate electrocatalytic properties in ORR in acidic electrolytes and the prevailing process herewith, according to the two-electron oxygen reduction with the formation of hydrogen peroxide. The CP dopant was chosen to be 12-phosphomolybdic acid, $H_3PMo_{12}O_{40}$ (PMA) that features the highest

electrocatalytic activity in ORR among the unsubstituted Keggin- or Dawson-type HPAs [11].

Importantly, PAni-inorganic oxide nanocomposites are effective electrocatalysts for many reactions and have been employed in sensor applications [12, 13]. PAni/WO_3 composites have been prepared and used as humidity sensor [14]. The heterogeneous branched core–shell SnO_2–PAni nanorod arrays have been designed and fabricated by an efficient and facile hydrothermal treatment followed by electrodeposition [15]. Phosphomolybdic acid-doped PAni/V_2O_5 composite has been proved to be an effective electrocatalyst in oxygen reduction in weakly acidic solution. Metal oxides such as M_OO_3 and VO_2 offered electrocatalytic properties when incorporated into PAni matrix [16–18]. Electroactivity of the NiO(x)/POT(y) (x = amount of NiO-NPs (mg), y = concentration of OT (mM)) films showed dependence on x and y. Efficient electrocatalysts could be obtained by tuning of x and y was reported by Komathi et al. [19]. Gang Wu et al. reported that the nitrogen-doped TiO_2-supported PAni-Fe catalyst exhibits much improved catalytic activity for oxygen reduction when compared to the traditional carbon-supported materials [20].

Thus, the aim of this work was to study the regularities of electrochemical and electrocatalytic behaviour in the ORR of the hybrid nanocomposites based on CP and nanosize ceramic. Their methanol reduction in different atmospheric conditions is also studied.

Methods

UV–Vis spectra of the samples were recorded on a JASCO V530 UV–Vis spectrophotometer. Fourier transform infrared spectroscopy (FTIR) (Model: SHIMADZU) of polyaniline–TiO_2 nancomposites (PAniTNCs) was studied in the frequency range of 400–4000 cm^{-1}. X-ray diffraction (XRD) was carried out with the Bruker AXS D8 Advance using CuK_α radiation source energized at 40 kV (λ = 0.154 nm). Samples were scanned at a rate of 29.5° per sec where 2θ ranges from 1° to 80°. Morphological study of the PAniTNCs was carried out using scanning electron microscopy (SEM Model: JEOL JSM 6360) operated at 25 kV. The structure of the PAniTNC was confirmed using transmission electron microscopy (TEM) (PHILIPS Model CM200) operated at 20–200 kV with resolution of 2–4 Å. Differential scanning calorimetry (DSC) studies were carried out using METTLER Toledo DSC operated at −150 to 700 °C. Thermogravimetric analysis (TGA) studies were carried out using Perkin Elmer Thermal Analysis in which operating temperature ranges between 40.00 and 960.00 °C at a rate of 20.00 °C/min. Cyclic voltammetry, chronoamperometry and chronocoulometry studies were carried out in the presence of nitrogen and oxygen atmosphere, and impedence spectroscopy was also experimented using CH Instrument (Model 650C) Electrochemical workstation.

Results and discussion

XRD studies

X-ray diffraction patterns were recorded for the prepared samples of PAniTNCs and a comparison was made between them as shown in Fig. 1a–f. The XRD pattern of PAni shows a broad peak at 2θ whose resultant value indicates 25.30° which corresponds to the (110) plane of PAni. It reveals that PAni is amorphous in nature which may be assigned to the scattering of PAni chains at interplanar spacing. When $K_2S_2O_8$ is added to the reaction system, it is observed that polymerization proceeds initially on the surface of TiO_2 nanoparticles due to the restrictive effect of the surface. Thereafter, polyaniline encapsulates the crystalline behaviour of TiO_2 thus hampering its crystalline behaviour. Therefore, the degree of crystallinity of polyaniline decreases, and the diffraction peaks emerge with TiO_2 peaks and hence cannot be distinguished. By comparing the XRD patterns of TiO_2–PAni nanocomposite with that of PAni, it was found that the prominent peaks corresponding to 2θ = 25.61°, 38.12°, 47.53° and 54.03° are due to (110), (101), (111) and (211) crystal planes of

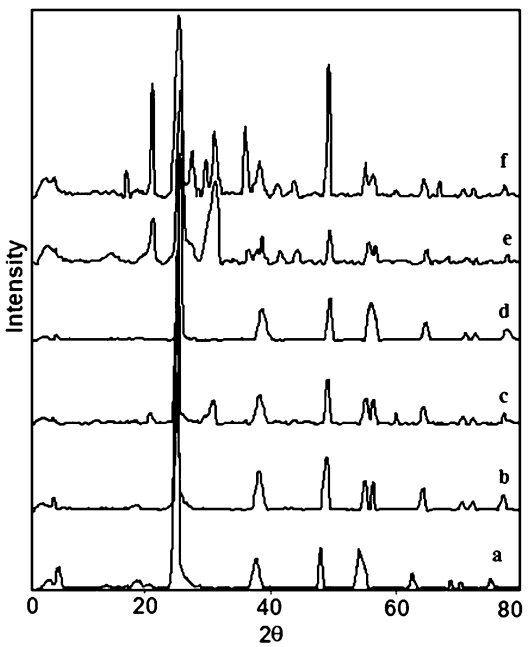

Fig. 1 X-ray diffractogram of PAniTNCs (*a* PAniTNC1, *b* PAniTNC2, *c* PAniTNC3, *d* PAniTNC4, *e* PAniTNC5 and *f* PAniTNC6)

anatase TiO_2 which indicate the presence of TiO_2 in PAni [JCPDS file no. 21-1276]. It is observed that TiO_2 has retained its structure even though it is dispersed in PAni after polymerization reaction [21]. The very sharp intensity peaks obtained for PAniTNC5–PAniTNC6 are not so in the case of PAniTNC1–PAniTNC4 as the peaks are suppressed due to the conducting emaraldine base of PAni.

SEM, EDX and TEM studies

Figure 2a–f shows the SEM images of PAniTNC1–PAniTNC6. It can be seen that the morphology of composites for low contents of TiO_2 i.e. 0.25, 0.50, 0.75 and 1.0 g of TiO_2 is much similar to that of polyaniline. Especially, PAniTNC1 (0.25 g) shows some fibrous microstructure due to the very low composition of TiO_2 nanoparticles. The change in surface morphology has been observed with the increasing content of TiO_2 (0.25–1.50 g) in PAni. The encapsulated TiO_2 particles in the PAni matrix have changed from sponge-like structure (PAniTNC1) to granular flower (PAniTNC6) structure. As the composition of TiO_2 increases, agglomeration and uneven distribution of TiO_2 particles can be seen in the PAni matrix. The diffraction pattern from the edge of particles of PAniTNC1–PAniTNC6 suggests that the TiO_2 nanoparticles are deposited on the surface of PAni and show typical anatase phase, and this agrees well with the X-ray diffraction result of TiO_2 nanoparticle sample [22]. The EDX analyses of the PAniTNCs are also performed in order to confirm the incorporation of the TiO_2-nanoparticles in the PAni matrix. Intensity of the peak is found to increase gradually while increasing the ceramic amount.

TEM images of the nanocomposite are presented in Fig. 3. In Fig. 3a, aggregation with spherical structures is found obviously and the spherical aggregates are composed of dark spots. As shown in Fig. 3a, the dark spots symbolising TiO_2 nanoparticle are encapsulated with PAni matrix for PAniTNC1 and are found to be larger than the particle size obtained from XRD results. The particle size of ceramic nanomaterial is observed and ranges between 29.6 and 123.6 nm as shown in Fig. 3a. Therefore, it is considered that the aggregates of TiO_2 nanoparticles exist within the PAni matrix. Figure 3b shows the electron diffraction pattern of PAniTNC1.

DSC studies

Differential scanning calorimetry (DSC) of PAniTNC1–PAniTNC6 samples is shown in Fig. 4a–f and Table 1. The first peak appeared in the temperature range of 67–112 °C which may be inferred as the release of moisture. Second peak appeared in the range of 121–212 °C. This may be attributed to the degradation of polymer functionalities. The third peak appeared in the range of 210–262 °C which may be assigned to the release of loosely bounded polymer molecule in nanocomposites. The fourth peak value is obtained above 300 °C in PAniTNC4–PAniTNC6 due to nanocomposites. These thermal data indicate the softening of polyaniline on addition of TiO_2 thus enhancing their thermoplasticity and thermoprocessing. These results prove the greater thermal stability of the nanocomposite due to the attractive coulombic interaction between the positive group of PAni layer and negatively charged surface of the TiO_2 layer. PAniTNC1 exhibits only two weight losses which is indicative of the low amount of TiO_2 and hence is stable.

TGA and DTA studies

The TGA of PAniTNCs samples is shown in Fig. 5a–f and Table 2. The first step (85–98 °C) may be assigned to the loss of moisture. In the second step (299–322 °C), elimination of the polymer is expected. The result agrees with the evaporation of moisture which is trapped inside the polymer or bound to the polymer backbone as evidenced by the degradation stage of TGA curve [23]. The third weight loss starting from ~760 to 832 °C could be correlated to the thermal decomposition of the nanocomposite [24]. The PAniTNC1–PAniTNC6 matrix shows residual weights around 20 % at 916 °C. Figure 5a (PAniTNC1) shows that it was stable up to 832 °C, when compared to PAniTNC2–PAniTNC6 as well as PAni. The temperatures get gradually decreased while increasing the ceramic content in the PAni matrix. Thus, it could be concluded that PAniTNC1 is thermally stable.

FTIR studies

The important characteristic peaks observed in FTIR spectra of PAniTNCs are shown in Table 3 and Fig. 6a–f. The origins of the vibration bands are as follows: The stretching frequency at 3431–3456 cm^{-1} is due to the NH of aromatic amine. Those from 2852 to 2923 cm^{-1} are due to aromatic CH stretching vibration, and CH out-of-plane bending vibration was observed at 505 cm^{-1}. The CH out-of-plane bending mode has been used as a key to identify the type of substituted benzene. The bands of PAni at 1558, 1577–1581 and 1481–1485 cm^{-1} are attributed to C=N and C=C stretching modes of vibration for the quinonoid and benzenoid units of polyaniline. The peaks at 1298–1301 and 1242–1245 cm^{-1} are assigned to the C–N stretching of benzenoid ring. The peak at 1242 cm^{-1} is characteristic of the conducting protonated form of polyaniline. The bands in the region 1114–1126 cm^{-1} are due to in-plane bending vibrations of C–H mode of N=Q=N, Q=N + H=B and B–N + H–B, which is formed

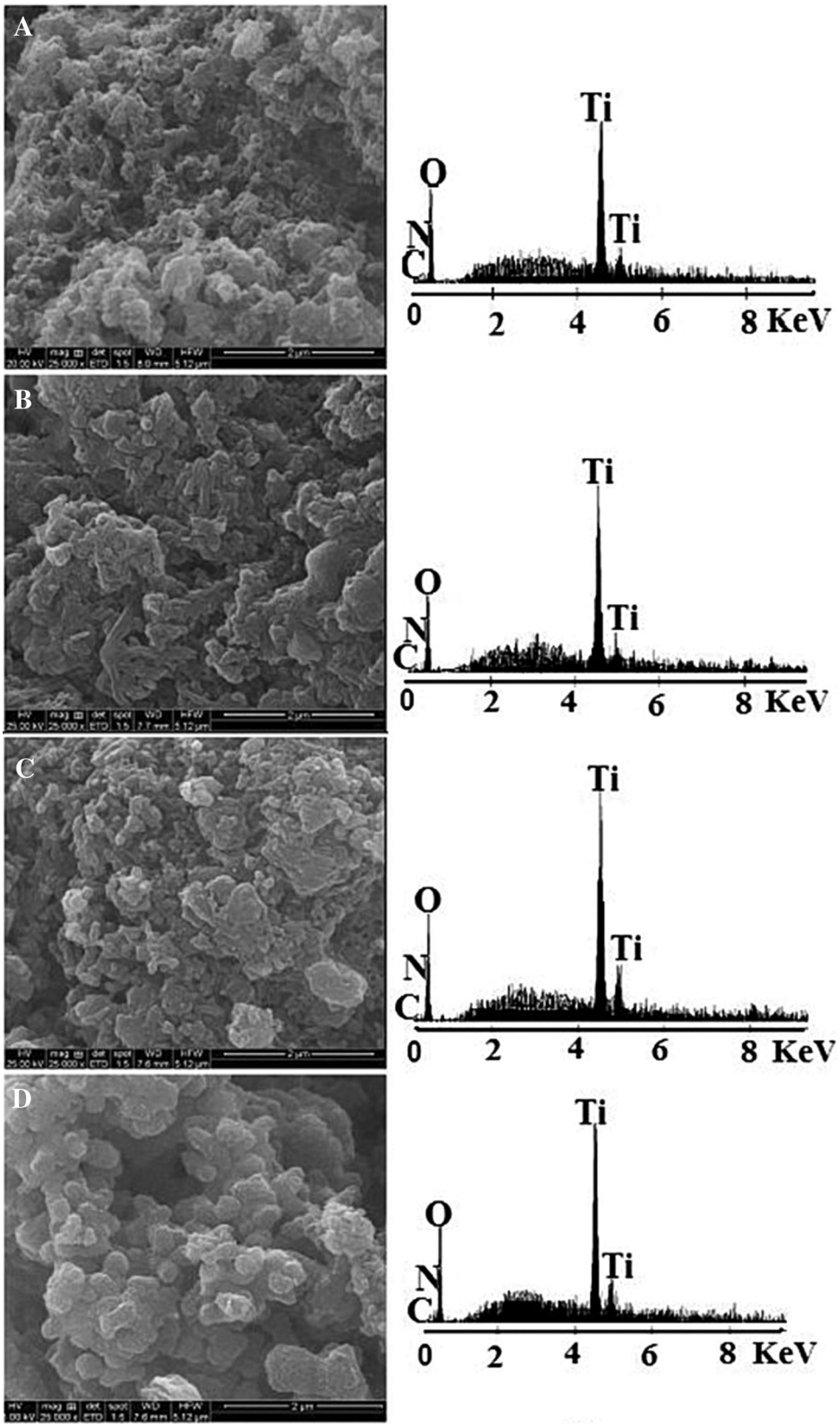

Fig. 2 SEM and EDX of PAniTNCs (**a** PAniTNC1, **b** PAniTNC2, **c** PAniTNC3, **d** PAniTNC4, **e** PAniTNC5 and **f** PAniTNC6

Fig. 2 continued

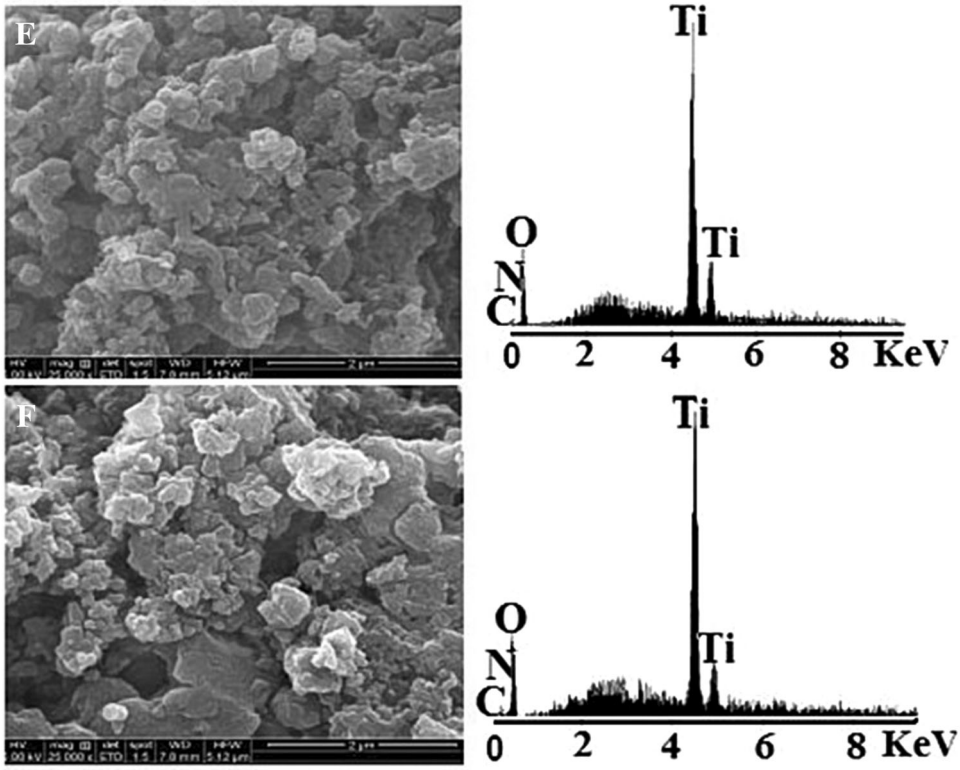

during protonation [25]. The band at 798–804 cm^{-1} originates from the out-of-plane C–H bending vibration. The low-wavenumber region exhibits a strong vibration around 725 cm^{-1} which corresponds to the anti-symmetric Ti–O–Ti. When compared with PAni, certain changes were observed in intensity and wavelength shifts due to changes in π electron delocalisation in the aromatic rings; the shift towards higher wavenumber indicates an increase in the conjugation length as a result of doping with an electron-rich dopant. Both the amine and imine groups of PAni are affected by dopant, thus changing the wave number of both C–C and C=N stretching. These red-shifted peaks may also be due to PAni transition from the emeraldine base (EB) to the emeraldine salt (ES) during the doping process or morphological changes [26]. These results confirm that structural and morphological changes occurred in PAni. IR spectral peak value confirms the formation of PAni–titania nanocomposites.

UV–Vis studies

Prepared PAni–TiO_2 nanocomposites were studied by UV–Vis absorption spectroscopy with λ ranging from 1100 to 200 nm. The absorption spectra thus obtained incorporating various ratios of TiO_2 used in PAniTNCs are shown in Fig. 7a–f. The electronic spectra of PAniTNCs exhibited bands at ~272 and ~368 nm which are attributed to π–π^* transitions in the benzenoid structure [27]. The peak at about 610 nm has been shifted to lower wavelengths of ~558 nm which may be due to the n–π^* transitions of quinine–imine groups [28]. These results showed that PAni was completely converted from emeraldine salt to the emeraldine base form by the deprotonation of PAni with NH_4OH [29].

The intensity of peaks alters with different concentrations of ceramic content. Figure 7a indicates that insertion of nano-TiO_2 particles led to doping of the conducting polyaniline, and hence led to an interaction at the interface of polyaniline and nano-TiO_2 particles [30, 31]. It has been noticed that these peaks PAniTNC1 shift towards lower intensity when there is a change in ceramic amount (0.5, 0.75, 1.0, 1.25 and 1.5 g). This may be due to interchain species, which play an important role in the process of conjugated polymers. The strong interactions between the PAni chains create conjugation defects leading to a compact coil conformation. As the TiO_2 content is increased (Fig. 7b–f), a free carrier tail is observed in the visible region, which is consistent with the delocalization of polorons [25] promoted by extended chain conformation of PAni.

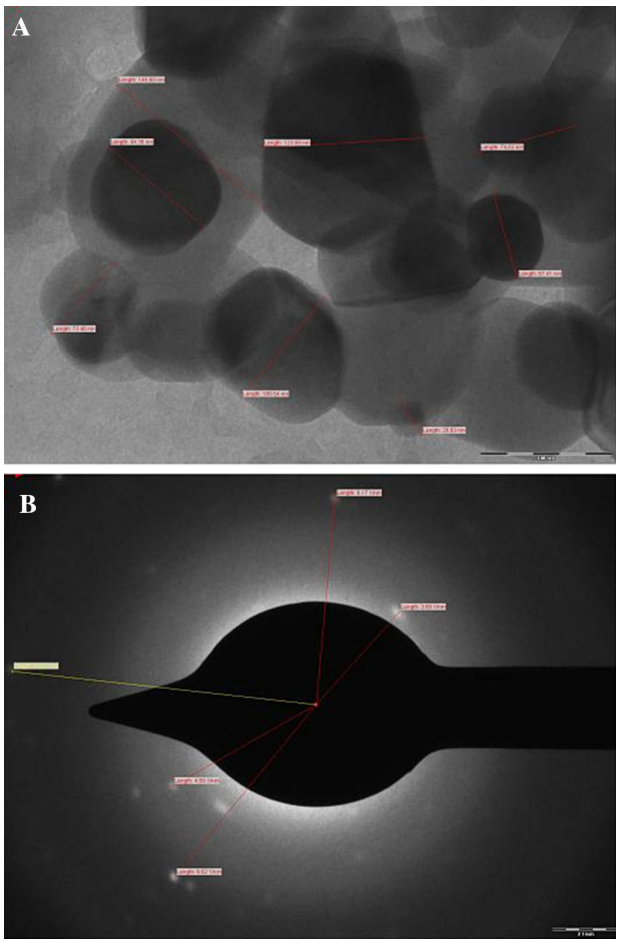

Fig. 3 **a** Transmission electron micrographs of PAniTNC1 and **b** electron diffraction pattern of PAniTNC1

Electrochemical characterization

Cyclic voltammetry

PAniTNC1-modified glassy carbon electrodes were employed in the present investigation. It was dissolved in dimethyl sulfoxide (DMSO) to form polymer–ceramic nanocomposite solution. PAniTNC1 films were produced by casting the solutions (1 drop) onto a clean and pre-treated 0.0314 cm^2 GCE and then allowing the solvent to evaporate. They were consequently rinsed with water and then transferred to an electrochemical cell for experimental purpose. A three electrode cell with a saturated calomel reference electrode (SCE), a platinum wire counter electrode and PAniTNC1-modified glassy carbon working electrode was employed. All electrochemical experiments were carried out at a thermostatic temperature of 25.0 ± 2 °C.

Cyclic voltammetric studies of PAniTNC1-modified GCE were performed for different pH, different concentrations and different atmospheric (N_2 and O_2 gases) conditions. The CVs were obtained in 1.0 M H_2SO_4 electrolyte by casting the nanocomposite on GC working electrode and scanned between −1.2 and 1.2 V at scan rates from 50 to 500 mV/s.

The effect of different concentrations of PAniTNCs on the voltammetric response was studied as shown in Fig. 8a. The high peak current appeared for PAniTNC1 when compared with other PAniTNCs. Thus, the current of PAniTNC1-modified GCE increases with the addition of TiO_2 (0.25 g TiO_2) and decreases with a further increase in TiO_2. This result clearly shows that the increases the current density with decreasing the amounts of TiO_2, because conducting polymer matrix is replaced gradually by ceramic. Thus PAniTNC1 gives better voltammetric response and which was chosen for subsequent studies.

Influence of pH

The effect of pH on voltammetric response of PAniTNC1 was studied on modified GCE in the pH range of 1.0–13.0, using pH buffer solutions adjusted to the desired condition which is illustrated in Fig. 8b. Background current or capacitative current is generally pH dependent. When the pH of the solution is greater than seven, PAniTNC1 becomes non-electroactive. The indication of lesser electroactivity is due to the failure of the formation of the emeraldine salt (ES) with titania nanocomposites. The surface of TiO_2 particles has zero charge at pH 7. This could be made to acquire positive charge in acidic condition by the addition of H_2SO_4 (pH 1–3). Thus, the Cl^- ions get adsorbed on the positively charged TiO_2 particles which would work as a charge compensator for positively charged PAni chain in the formation of PAni–TiO_2 nanocomposites [32]. The optimum pH range for good sensitivity response appears to be 1.0.

Effect of different atmospheres

The voltammograms for PAniTNC1-modified GCE in 1.0 M H_2SO_4 were obtained in normal as well as N_2- and O_2-saturated buffer. These voltammograms are demonstrated in Fig. 8c. Cyclic voltammograms depict a well-defined pair of oxidation–reduction observed on modified GCE at 50 mV/s.

The cyclic voltammogram of PAniTNC1-modified GCE presented in Fig. 8c shows an oxidation peak at +565.9 mV and a broad reduction peak which started from +683.7 to +326.7 mV under normal condition. PAni–TiO_2

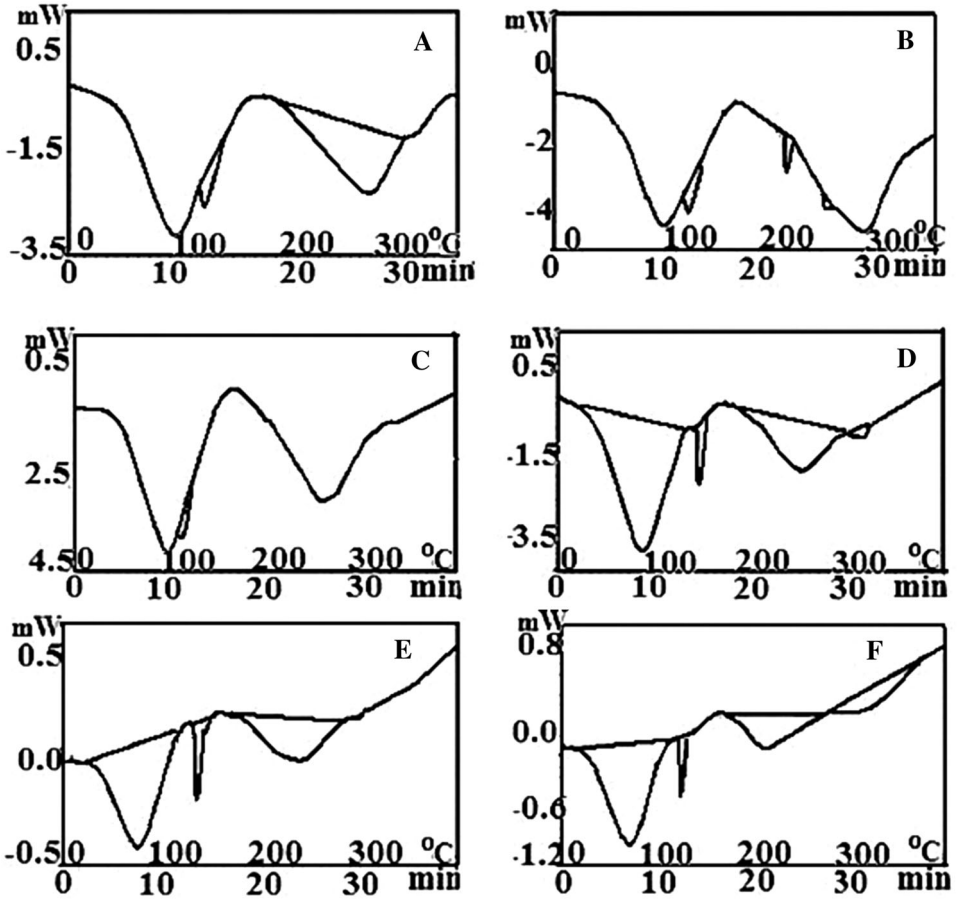

Fig. 4 DSC of PAniTNCs (**a** PAniTNC1, **b** PAniTNC2, **c** PAniTNC3, **d** PAniTNC4, **e** PAniTNC5 and **f** PAniTNC6)

Table 1 DSC values of PAniTNC1–PAniTNC6

PAniTNCs	First peak (°C)	Second peak (°C)	Third peak (°C)	Fourth peak (°C)
PAniTNC1	112.89	–	262.4	–
PAniTNC2	112.5	206.3	262.29	–
PAniTNC3	109.85	190.3	251.1	–
PAniTNC4	84.87	143.7	249.73	318.26
PAniTNC5	71.3	131.8	235.17	302.0
PAniTNC6	67.96	121.3	210.8	322.68

shows better electrochemical catalytic activity. Under N_2-saturated buffer, it shows an oxidation peak at +469.3 mV and a broad reduction peak from +730.1 to +290.9 mV. At O_2-saturated buffer, two oxidations at +330.1, +672.8 mV and reduction at +558.7, +162.4 mV are observed. The presence of an additional peak could be related to the degradation product (quinine/hydroquinone couple) [33]. PAniTNC1-modified GCE shows a larger enhancement in the anodic and cathodic current peak and electro-oxidation peak shifted towards lower potential (~130 mV) and the electro-reduction peak potential shifted towards the negative side (~180 mV), when compared with N_2-saturated buffer. The change in conductivity is accounted for the interaction between O_2 and PAni which loses and gains electrons in valence band in the presence of TiO_2 [34]. The result clearly shows that PAniTNC1 has electrocatalytic redox behaviour enhanced under O_2-saturated buffer.

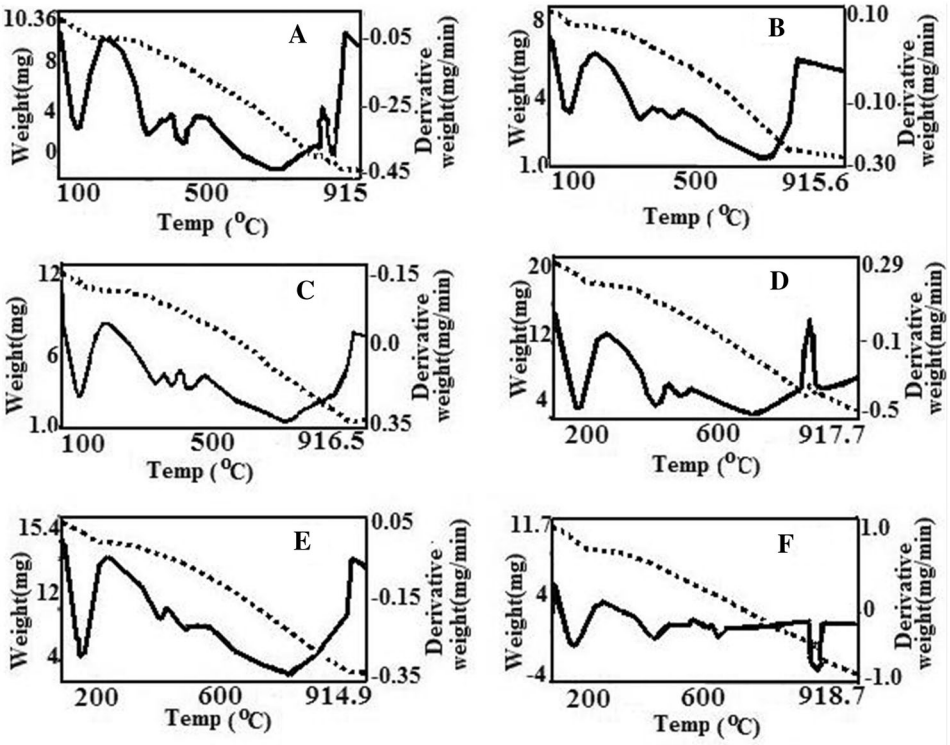

Fig. 5 TGA/DTA curves of PAniTNCs (**a** PAniTNC1, **b** PAniTNC2, **c** PAniTNC3, **d** PAniTNC4, **e** PAniTNC5 and **f** PAniTNC6)

Table 2 TG/DTA data for the nanocomposites temperature (°C)

Sample	First step	Second step	Third step
PAniTNC1	91	300, 393	832
PAniTNC2	85	299	760
PAniTNC3	87	305	784
PAniTNC4	92	319	774
PAniTNC5	89	312	–
PAniTNC6	98	322	790

Effect of scan rate

The effect of varying scan rates from 50 to 500 mV/s was studied at the PAniTNC1-modified GCE in 1 M H_2SO_4. With increasing the scan rate, the peak current separation increased, and also the peak potential shifted slightly with the anodic peak to positive and the cathodic peak to negative potential directions. This is because the charging and discharging of the electroactive CP determines the rate. Figure 8d shows the plot of logarithm peak current against logarithm of scan rate, which clearly indicates that the current increases approximately in linear approach as described by the equation, $y = 0.596x - 1.1755$; $R^2 = 0.9933$ for the anodic peak currents. This also shows good adherence of the composite onto the electrode surface. The experimental slope value of 0.596 was found to be greater than the theoretical value of 0.5, which suggests that process is purely adsorbtion controlled.

Chronoamperometry studies

Chronoamperometric studies were performed on PAniTNC1-modified GCE with normal, N_2- and O_2-saturated buffer with an initial and final potential of −1.6–1.4 V versus SCE. Figure 9 shows that the PAniTNC1-modified GCE current was high in O_2-saturated buffer which is however less in the case of normal and N_2-saturated buffer. Thus, the O_2 gas interfered with the nanocomposite layer and enhanced the current.

From the slope value obtained by the plot of I versus $t^{-1/2}$, the diffusion coefficient values of PAniTNC1-modified GCE were determined by Cottrell equation. The calculated surface coverage (N_p) and diffusion coefficient (D) values are tabulated in Table 4. The D and N_p values are very higher for O_2-saturated buffer in comparison to those for the normal and N_2-saturated buffer.

Chronocoulometry studies

Chronocoulometric behaviour of PAniTNC1-modified GCE was investigated in the absence and presence of N_2-

Table 3 Characteristic frequencies of PAniTNC1–PAniTNC6

PAniTNC1	PAniTNC2	PAniTNC3	PAniTNC4	PAniTNC5	PAniTNC6
3431	3433	3446	3449	3455	3456
2852	2852	2854	2854	2923	2923
1577	1579	1577	1577	1581	1577
1481	1477	1481	1485	1481	1481
1298	1298	1298	1298	1299	1301
1242	1242	1245	1245	1245	1244
1114	1116	1112	1120	1122	1126
798	800	802	800	804	802
721	723	724	724	726	725
505	505	505	505	505	505

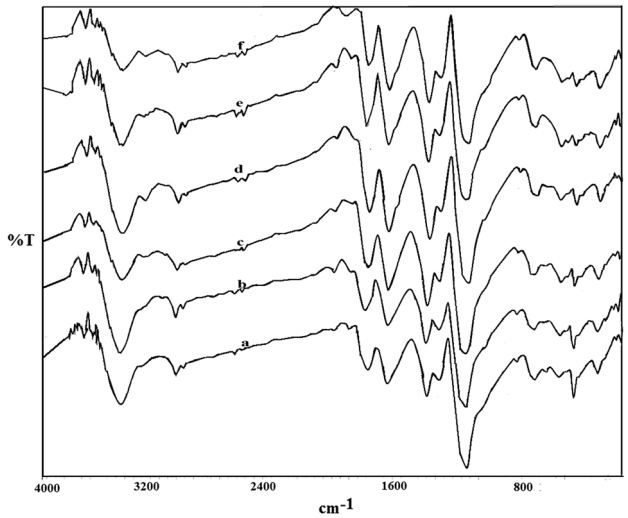

Fig. 6 FTIR spectra of PAniTNCs (*a* PAniTNC1, *b* PAniTNC2, *c* PAniTNC3, *d* PAniTNC4, *e* PAniTNC5 and *f* PAniTNC6)

and O_2-saturated buffer by performing a double potential step technique with initial and final potential of −1.4–1.2 V versus SCE (Fig. 10). PAniTNC1-modified GCE immersed in 1.0 M H_2SO_4 at 25 ± 2 °C for 2 s shows a large enhancement in charge in O_2-saturated buffer when compared to N_2 and normal buffer, indicating that the nitrogen and oxygen buffer interferes with the nanocomposite layer, thereby increasing the charge. It has been previously confirmed by cyclic voltammetry and chronoamperometric techniques. The Anson plot shows linear dependency of Q upon $t^{1/2}$ indicating that the process involved adsorption controlled for normal condition as well as O_2- and N_2-saturated buffer solution.

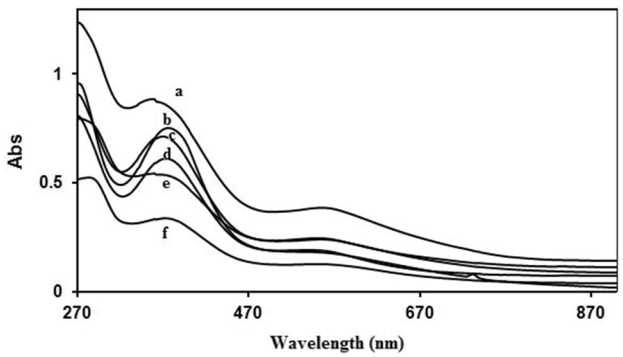

Fig. 7 UV–Vis spectra of PAniTNCs (*a* PAniTNC1, *b* PAniTNC2, *c* PAniTNC3, *d* PAniTNC4, *e* PAniTNC5 and *f* PAniTNC6)

Effect of pH in the presence of methanol

PAniTNC1-modified GCE shows enhanced electrocatalytic activity in 1.0 M H_2SO_4 (pH1) which slightly increases in the case of O_2-saturated buffer. For this reason, linear sweep voltammetry has been recorded in 1.0 M H_2SO_4 and 1.0 M MeOH (acidic methanol), on PAniTNC1-modified GCE. It was carried out in normal as well as O_2- and N_2-saturated in methanol at 50 mV/s shown in Fig. 11. The LSV shows a broad reduction peak from +698.6 to +303.8 mV for normal and N_2 atmospheric condition and two reduction peaks at +522.9 and +208.8 mV for O_2 medium. PAniTNC1-modified GCE shows a larger enhancement in the cathodic peak current and potential shifted towards the negative side (lower potential) under O_2 condition, suggesting good electrocatalytic behaviour. The results clearly show that PAniTNC1-modified GCE enhances electrocatalytic reduction (ORR activity) behaviour towards methanol under O_2-saturated acidic metha-

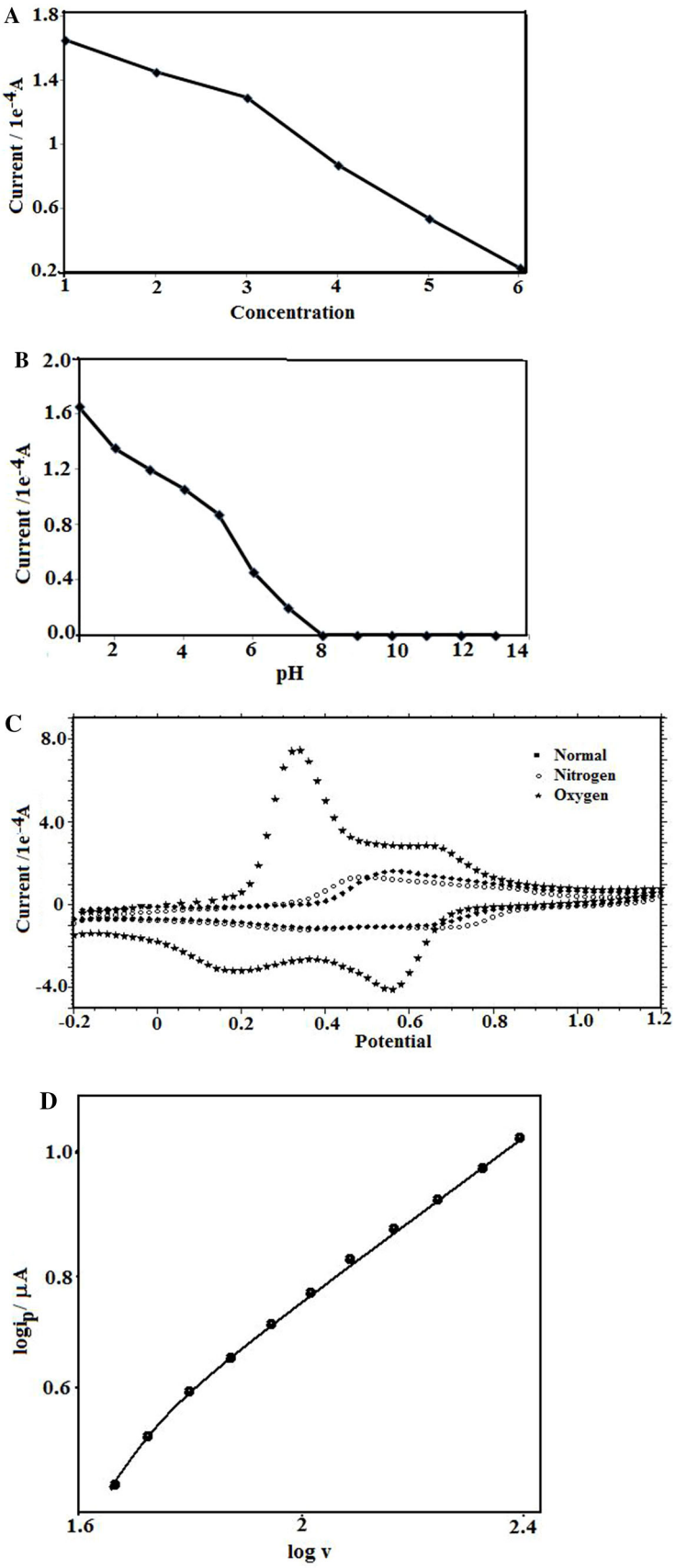

Fig. 8 **a** Plot of concentration versus current (*1* PAniTNC1, *2* PAniTNC2, *3* PAniTNC3, *4* PAniTNC4, *5* PAniTNC5 and *6* PAniTNC6). **b** Plot of pH versus current. **c** Cyclic voltammetric responses obtained for PAniTNC1-modified GCE in the presence of pH 1.0 with a scan rate of 50 mV/s. **d** Plots of logarithm of scan rate versus logarithm peak current

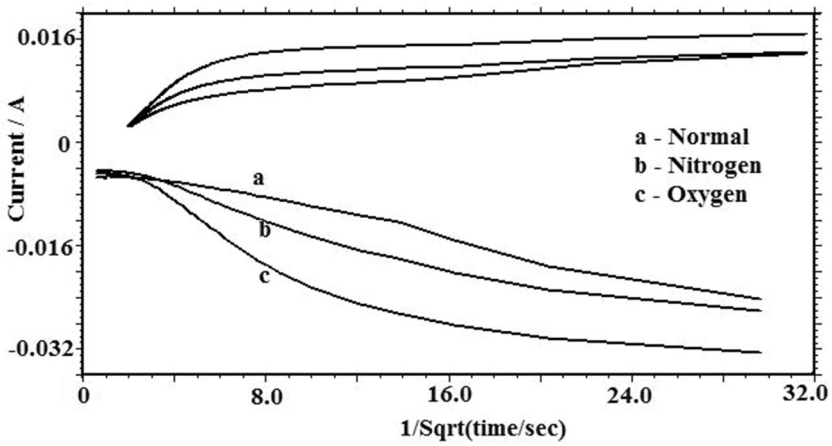

Fig. 9 Chronoamperogram of PAniTNC1 GCE at 25 ± 2 °C with 250 ms

Table 4 Surface coverage (N_p) and diffusion coefficient of responses obtained for PAniTNC1-modified GCE

PAniTNC1	N_p (mol/cm^2)	D (cm^2/s)
Normal	4.0929×10^{-4}	2.9635×10^{-6}
N_2	5.5122×10^{-4}	6.5829×10^{-6}
O_2	1.208×10^{-3}	1.68913×10^{-5}

nol compared to that in pH 1.0 solution. The methanol reduction mechanism is given below.

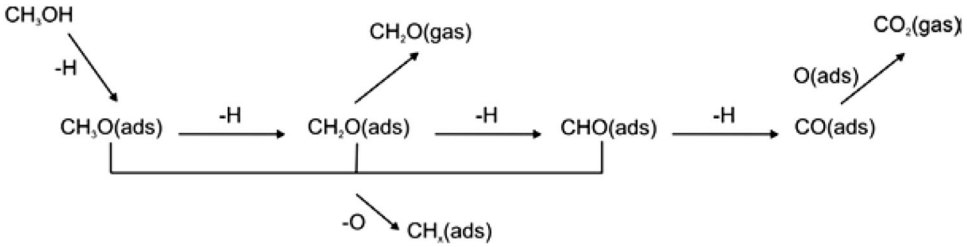

equals the charge-transfer resistance (R_{ct}) through PAni/TiO_2 composite. Smaller R_{ct} indicates a faster electron-transfer rate. The radii of the semicircle of PAniTNC1–PAniTNC6 (3.211×10^3–9.066×10^3) are found to increase with the increase in ceramic concentration which shows greater resistance to conduction with increase in ceramic concentration.

These values clearly indicate that a decrease in the capacitance values increases the resistance to Faraday current. Hence it can be concluded that the high conductivity of the nanocomposite with lower ceramic concentration (PAniTNC1) could enhance the electron-transfer rate. PAniTNC2–PAniTNC6 conductivity decreased gradually, while increasing the ceramic content. It is supported by UV and XRD studies.

Electrochemical impedence spectroscopy (EIS) studies

Electrochemical impedance measurements were carried over a frequency range from 1000 to 0.01 Hz in open circuit potential. Figure 12 shows the electrochemical impedance spectra (Nyquist plots, Z' vs. Z'') for PAniTNC1–PAniTNC6-modified GCE in 1.0 M H_2SO_4. The C_{dl} values of PAniTNC1–PAniTNC6 are given as follows: 3.442×10^{-8}, 8.48×10^{-8}, 2.69×10^{-9}, 4.115×10^{-9}, 4.6509×10^{-9} and 5.09×10^{-9} F/cm^2. The semicircle at high frequencies was characteristic of the charge-transfer process and the diameter of the semicircle

Experimental

The aniline used was of analytical reagent (AR) grade from Sigma–Aldrich Co. Aniline was purified by distillation under vacuum before use. The PAniTNC nanocomposites were prepared by keeping the concentration of the monomer and oxidant constant and varying the wt% of ceramic

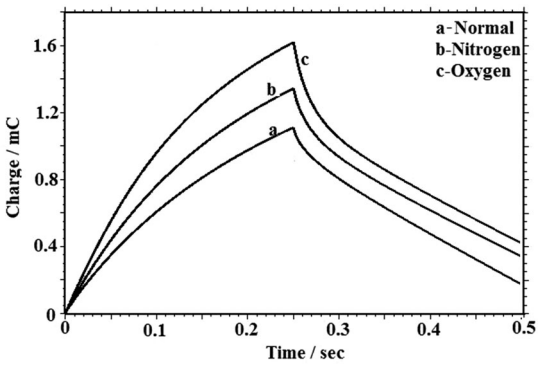

Fig. 10 Chronocoulomogram of PAniTNC1 GCE at 25 ± 2 °C with 250 ms

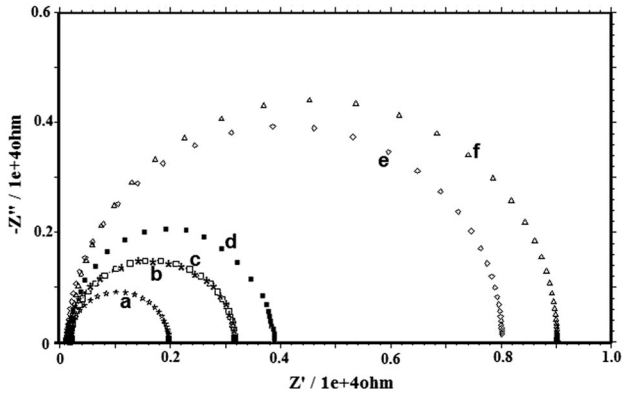

Fig. 12 Electrochemical impedance spectra of *a* PAniTNC1, *b* PAniTNC2, *c* PAniTNC3, *d* PAniTNC4, *e* PAniTNC5 and *f* PAniTNC6-modified GCE/TiO_2/PAni electrode in the presence of 1 M H_2SO_4 (pH 1.0)

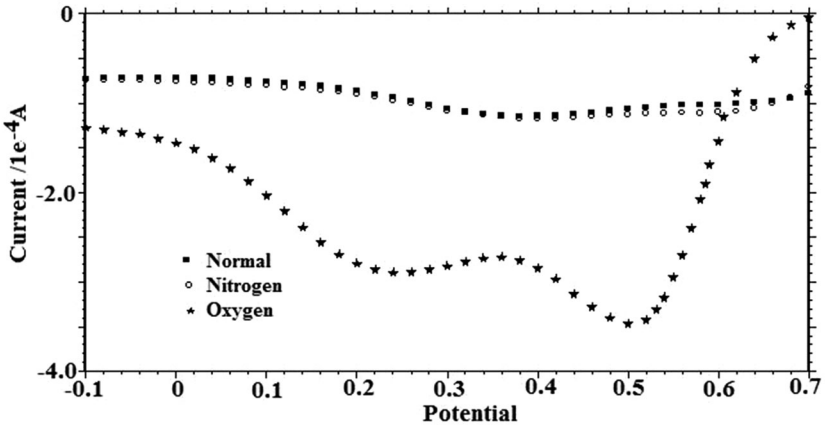

Fig. 11 Linear sweep voltammetric cathodic peak obtained for PAniTNC1-modified GCE in the presence of acidic methanol with a scan rate of 50 mV/s

from 0.25 to 1.5 g (0.25, 0.5, 0.75, 1.0, 1.25, 1.5 g). Bulk polymerization was carried out by mixing various weight percents of ceramic into a mixture of 9 ml of 0.5 M aniline and 6 ml of 1 M hydrochloric acid and made up to 200 ml using conductivity water. To this the oxidant viz., potassium perdisulphate was added with constant stirring. The nanocomposite temperature ≈0 °C was maintained for 24 h to complete the reaction. Then the precipitate was filtered and washed successively using distilled water until the wash solution turned colourless. The nanocomposite was dried in room temperature. The CP nanocomposites synthesized were designated as PAniTNCP1 to PAniTNC6.

Conclusions

The various amount of TiO_2 used polyaniline–TiO_2 nanocomposites was synthesized successfully. The better results were obtained for lower concentration TiO_2 used nanocomposites. Synthesised nanocomposites were analysed through UV-Vis and FTIR spectra. PAni–TiO_2 nanocomposites are in nanoscale, which is confirmed by XRD and TEM. SEM images showed that sponge-like morphology gradually changed into granular flower-like morphology. Ceramic content ratio was proved by EDX studies. Thermal stability of the PAniTNC was studied by TGA and DSC analyses. In electrochemical studies, PAniTNC1-modified GCE shows electrocatalytic redox behaviour under O_2-saturated buffer at pH 1.0. Especially, the reduction behaviour is enhanced for acidic methanol solution when subject to O_2-saturated buffer than N_2-saturated buffer and normal condition. Voltammograms show that redox reaction of PAniTNC1 is adsorption controlled. The diffusion coefficient value is high in the case of O_2-saturated buffer. This has also been depicted by chronoamperometric and chronocoulometric studies. EIS study also showed that PAniTNC1 exhibits good conductivity.

Acknowledgments The authors are extremely grateful to DST (FAST TRACK and FIST) New Delhi, INDIA for providing CHI Electrochemical workstation and Jasco UV–Vis Spectrophotometer.

Authors' contributions PR carried out synthesis and all experimental works. CV monitored all the works. Authors have read and approved the final manuscript.

Conflict of interest The authors declare that they have no competing interests.

References

1. Bashyam R, Zelenay P (2006) A class of non-precious metal composite catalysts for fuel cells. Nature 443:63–66
2. Podlovchenko BI, Andreev VN (2002) Electrocatalysis on polymer modified electrodes. Usp Khim 71:950–966
3. Khomenko VG, Barsukov VZ, Katashinskii AS (2005) The catalytic activity of conducting polymers toward oxygen reduction. Electrochim Acta 50:1675–1683
4. Sadakane M, Steckhan E (1998) Electrochemical properties of polyoxometalates as electrocatalysts. Chem Rev 98:219–237
5. Hasik M, Pron A, Kulszewicz Bajer I, Pozniaczek A, Bielanski A, Piwowarska Z, Dziembaj R (1993) Polyaniline doped with heteropolyanions: spectroscopic and catalytic properties. Synth Met 55:972–976
6. Yu Posudievsky O, Kurys Ya I, Pokhodenko VD (2004) 12-Phosphomolybdic acid doped polyaniline-V_2O_5 composite. Synth Met 144:107–111
7. Kurys YI, Netyaga NS, Koshechko VG, Pokhodenko VD (2007) Polyaniline/12-phosphotungstic acid/V_2O_5 nanocomposite and its platinum analog as oxygen reduction electrocatalysts. Theor Exp chem 43:334–342
8. Tsujiko A, Itoh H, Kisumi T, Shiga A, Murakoshi K, Nakato Y (2002) Observation of cathodic photocurrents at nanocrystalline TiO_2 film electrodes, caused by enhanced oxygen reduction in alkaline solutions. Phys Chem B 106:5878–5885
9. Mentus SV (2004) Oxygen reduction on anodically formed titanium dioxide. Electrochim Acta 50:27–32
10. Kim JH, Ishihara A, Mitsushima S, Kamiya N, Ota KI (2007) Catalytic activity of titanium oxide for oxygen reduction reaction as a non-platinum catalyst for PEFC. Electrochim Acta 52:2492–2497
11. Stanis RJ, Kuo MCh, Ricket AJ, Turner JA, Herring AM (2008) Investigation into the activity of heteropolyacids towards the oxygen reduction reaction on PEMFC cathodes. Electrochim Acta 53:8277–8286
12. Min Y, Chen Y, ZhaoY Chen C (2008) Simple approach to synthesis Pt/NiO flower microspheres and their electro-catalytic properties. Mater Lett 62:4503–4505
13. Rashkova V, Kitova S, Konstantinov I, Vitanov T (2002) Vacuum evaporated thin films of mixed cobalt and nickel oxides as electrocatalyst for oxygen evolution and reduction. Electrochim Acta 47:1555–1560
14. Parvatikar N, Jain S, Khasim S, Revansiddappa M, Bhoraskar SV, Ambika Prasad MVN (2006) Electrical and humidity sensing properties of polyaniline/WO_3 composites. Sens Actuators B 114:599
15. Xu W, Zhao K, Niu C, Zhang L, Cai Z, Han C, He L, Shen T, Yan M, Qu L, Mai L (2014) Heterogeneous branched core-shell SnO_2-PANI nanorod arrays with mechanical integrity and three dimentional electron transport for lithium batteries. Nano Energy 8:196–204
16. Pan ZW, Dai ZR, Wang ZL (2001) Nanobelts of semiconducting oxides. Science 291:1947–1949
17. Law M, Kind H, Messer B, Kim F, Yang PD (2002) Photochemical sensing of NO_2 with SnO_2 nanoribbon nanosensors at room temperature. Angew Chem Int Ed 41:2405–2408
18. Pan ZW, Dai ZR, Wang ZL (2002) Lead oxide nanobelts and phase transformation induced by electron beam irradiation. Appl Phys Lett 80:309–311
19. Komathi S, Selvi P, Manisankar P, Gopalan AI, Lee KP (2011) Electrochemical properties of nickel oxide nanoparticles loaded poly(*o*-toluidine) composites. J Korean Electrochem Soc 14:56–60. doi:10.5229/JKES.2011.14.1.056
20. Gang Wu, Nelson Mark A, Mack Nathan H, Ma Shuguo, Sekhar Praveen, Garzona Fernando H, Zelenay Piotr (2010) Titanium dioxide-supported non-precious metal oxygen reduction electrocatalyst. Chem Commun 46:7489–7491
21. Parveen A, Roy AS (2013) Effect of morphology on thermal stability of core-shell polyaniline/TiO_2 nanocomposites. Adv Mater Lett 4:696–701
22. Guo Yanni, He Deliang, Xia Sanbao, Xie Xin, Gao Xiang, Zhang Quan (2012) Preparation of a novel nanocomposite of polyaniline core decorated with anatase-TiO_2 nanoparticles in ionic liquid/water microemulsion. J Nano Mater. doi:10.1155//202794
23. Narayan H, Alemu H, Iwuoha E (2006) Synthesis, characterization and conductivity measurements of polyaniline and polyaniline/fly-ash composites. Phys Status Solid A 203:3665–3672
24. Riaz Ufana, Ahmad Syed Aziz, Ahmad Sharif, Ashraf Syed M (2010) A comparative study on camphorsulphonic acid modified montmorillonite clay based conducting polymer nanocomposites. Polym Compos 31:906–912
25. Kang ET, Neho KG, Tan KL (1998) Polyaniline: a polymer with many interesting intrinsic redox states. Prog Polym Sci 23:277–324
26. Ram MK, Yavuz O, Lahsangah V, Aldissi M (2005) CO gas sensing from ultrathin nano-composite conducting polymer film. Sens Actuators B 106:750–757
27. Xia Y, Wiesinger M, MacDiarmid AG (1995) Camphor sulfonic acid fully doped polyaniline emaraldine salt: conformations in different solvents studied by an ultraviolet/visible/near-infrared spectroscopic method. Chem Mater 7:443–445
28. Rannou P, Gawlicka A, Berner D, Pron A, Nechtschein M, Djurado D (1998) Spectroscopic, structural and transport properties of conductive polyaniline processed from fluorinated alcohols. Macromolecules 31:3007–3015
29. Alam M, Ansari AA, Shaik MR, Alandis NM (2013) Optical and electrical properties studies of polyaniline/ZnO nanocomposite. J Nano Mater. doi:10.1155/2013/1578
30. Xia HS, Wang Q (2002) Ultrasonic irradiation: a novel approach to prepare conductive polyaniline/nanocrystalline titanium oxide composites. Chem Mater 14:2158–2165
31. Gospodinova N, Terlemezyan L (1998) Conducting polymers prepared by oxidative polymerization: polyaniline. Prog Polym Sci 23:1443–1484
32. Sathiyanarayanan S, Syed Azim S, Venkatachari G (2007) Preparation of PANI-TiO_2 composite and its comparative corrosion protection performance with PANI. Synth Met 157:205–213
33. Pawar SG, Patil SL, Chougule MA, Raut BT, Jundale DM, Patil VB (2010) Polyaniline:TiO_2 nanocomposites: synthesis and characterization. Arch Appl Sci Res 2:194–201
34. Huyen DN, Tung NT, Thien ND, Thanh LH (2011) Effect of TiO_2 on the gas sensing features of TiO_2/PANi nanocomposites. Sensors 11:1924–1931